

Lightweight equivariant interaction graph neural network for accurate and efficient interatomic potential and force predictions

Ziduo Yang^{1,2}, Xian Wang³, Yifan Li¹, Qiujie Lv^{1,2}, Calvin Yu-Chian Chen^{2,4,5,6,7*} and Lei Shen^{1*}

¹Department of Mechanical Engineering, National University of Singapore, 9 Engineering Drive 1, 117575, Singapore.

²Artificial Intelligence Medical Research Center, School of Intelligent Systems Engineering, Shenzhen Campus of Sun Yat-sen University, Shenzhen, 518107, China.

³Department of Physics, National University of Singapore, 2 Science Drive 3, 117551, Singapore.

⁴AI for Science (AI4S)-Preferred Program, Peking University Shenzhen Graduate School, Shenzhen, 518055, China.

⁵School of Electronic and Computer Engineering, Peking University Shenzhen Graduate School, Shenzhen, 518055, China.

⁶Department of Medical Research, China Medical University Hospital, Taichung, 40447, Taiwan.

⁷Department of Bioinformatics and Medical Engineering, Asia University, Taichung, 41354, Taiwan.

*Corresponding author(s). E-mail(s): cy@pku.edu.cn;
shenlei@nus.edu.sg;

Contributing authors: yangzd@mail2.sysu.edu.cn;
sunnywx623@163.com; e0576095@u.nus.edu;
lvqj5@mail2.sysu.edu.cn;

Abstract

In modern computational materials science, deep learning has shown the capability to predict interatomic potentials, thereby

supporting and accelerating conventional simulations. However, existing models typically sacrifice either accuracy or efficiency. Moreover, lightweight models are highly demanded for offering simulating systems on a considerably larger scale at reduced computational costs. A century ago, Felix Bloch demonstrated how leveraging the equivariance of the translation operation on a crystal lattice (with geometric symmetry) could significantly reduce the computational cost of determining wavefunctions and accurately calculate material properties. Here, we introduce a lightweight equivariant interaction graph neural network (LEIGNN) that can enable accurate and efficient interatomic potential and force predictions in crystals. Rather than relying on higher-order representations, LEIGNN employs a scalar-vector dual representation to encode equivariant features. By extracting both local and global structures from vector representations and learning geometric symmetry information, our model remains lightweight while ensuring prediction accuracy and robustness through the equivariance. Our results show that LEIGNN consistently outperforms the prediction performance of the representative baselines and achieves significant efficiency across diverse datasets, which include catalysts, molecules, and organic isomers. Finally, we conduct a comparative analysis of LEIGNN against both classical molecular dynamics (MD) and *ab initio* MD simulations across various systems, including solid, liquid, and gas. It is found that LEIGNN can achieve the accuracy of *ab initio* MD and retain the computational efficiency of classical MD across all examined systems, demonstrating its accuracy, efficiency, and universality.

Keywords: Graph Neural Networks, Equivariant Deep Learning, Interatomic Potentials and Forces, Molecular Dynamics

1 Introduction

In the field of computational materials science, the calculation of interatomic potentials is critical for obtaining energy and then other energy-related physical quantities, such as forces and atomic trajectories. The computational methods, using pre-fitted empirical functions to form interatomic potentials such as classical molecular dynamics (MD), provide very fast but low-accurate material-property calculations. Meanwhile, methods based on high-fidelity quantum-mechanics calculations, such as density functional theory (DFT) and *ab initio* molecular dynamics (AIMD), provide highly accurate energies and forces but require high computational costs.

To address the above dilemma, deep learning techniques, such as graph neural networks (GNNs), have been proposed for predicting interatomic potentials or DFT Hamiltonian in speed while preserving quantum mechanics-level accuracy[1–27]. To represent the molecule or crystal structure, GNNs typically use a graph where nodes are atoms and edges are chemical bonds between atoms. Atomic interactions are then simulated by graph convolution operations on the graph for passing message, where an atom can access its neighboring atoms during this process. By stacking multiple layers, GNNs can increase their accessible radius (or receptive field), enabling them to implicitly incorporate a wider range of interactions (Figure 1 (a)).

Currently, the most widely used GNNs are under the Euclidean group $E(3)$ *invariant* neural network architectures, which can effectively keep the crystal geometric symmetry and output energy with respect to $E(3)$ translations, rotations, and reflections. This is achieved by leveraging invariant features, such as bond lengths and angles, which remain constant under these transformations. Early models like CGCNN[4], SchNet[6], and MEGNet[7] primarily incorporate bond lengths, leading to challenges in distinguishing structures with identical bond lengths but different overall configurations, as shown in Figure 1 (b). Later iterations, like DimeNet[8], ALIGNN[9], and M3GNet[10], improve upon this by integrating bond angles. Despite this improvement, they still struggled to differentiate between structures sharing the same angles, as depicted in Figure 1 (c). Recent models, such as GemNet[1] and SphereNet[28], propose considering dihedral angles in GNNs to unambiguously recognize the local structures shown in Figure 1 (d). It is worth noting that distance and angular features are invariant representations which are only used to keep the geometric symmetry of crystals with respect to $E(3)$ transformations, rather than utilize the geometric symmetries in a more profound manner for increasing the prediction accuracy and the sample efficiency. Actually, the idea to leverage crystal symmetry for effectively describing the electron wave function and material properties was proposed a century ago. A physicist named Felix Bloch demonstrated a translation-symmetry-based structural function to maintain the equivariance of wave functions in 1928. Such an equivariant idea in crystals with periodic structures in 3D space provides a powerful framework for accurately understanding the material properties and significantly reduces the cost of computation, opening a new era for computational material science. Figures 1 (e), (f), and (g) offer a concise elucidation of invariance and equivariance in the context of predicting energy and forces.

In this work, we integrate equivariance into GNNs for actively exploiting crystal symmetries and offering a richer geometrical representation compared to their invariant counterparts. Most importantly, our equivariant network is lightweight, which only incorporates scalar and vector features and manipulates them in a manner that preserves symmetry, resulting in robust representations that enhance both accuracy and sample efficiency. Our lightweight equivariant interaction graph neural network (LEIGNN) is significantly different from previously reported equivariant GNNs which are on the

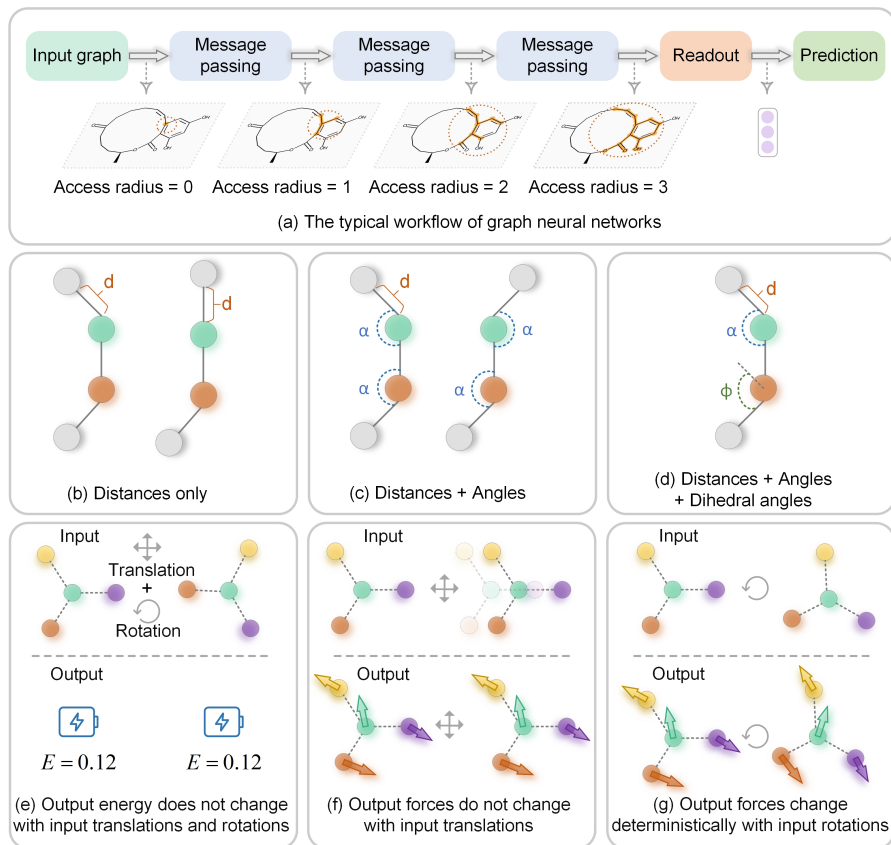


Fig. 1 Concepts of invariant GNNs. (a) A typical GNN workflow is illustrated, emphasizing how GNNs can include a wider range of interactions (or message passing) by stacking multiple layers to extend the accessible radius. (b), (c), and (d) underscore the importance of integrating structural features into GNNs, which include: (b) distance only, (c) both distance and angles, and (d) all distance, angles, and dihedral angles. (e), (f), and (g) elucidate the concepts of invariance and equivariance within the context of energy and forces prediction.

basis of high-order functions, such as the spherical harmonic function. Their increased accuracy compared with invariant GNNs initially came at the cost of increased computational expense [14, 21–23, 29–34]. Cutting-edge models like NequIP[14], ScN[34], and eScN[33] employ tensor product operations to combine input features and filters equivariantly, which is extremely expensive in practice computation [33–35].

Our model aims to achieve both accurate and efficient predictions for inter-atomic potentials and forces. Specifically, we assign each node both scalars and vectors to represent equivariant features. LEIGNN combines these entities in a symmetry-preserving fashion to maintain equivariance. Equivariant LEIGNN surpasses scalar-only invariant models[4, 6, 7] in accuracy and generalization ability. It also offers an extremely lightweight structure compared to high-order tensor models[14, 34]. The model’s performance is further enhanced by a novel

strategy for extracting global structural features from the vector representations. To validate the performance of our interatomic potentials, we conduct classical molecular dynamics and *ab initio* MD simulation across solid, liquid, and gas systems. LEIGNN can achieve the *ab initio* MD accuracy and computational efficiency of classical MD across all examined systems, showing its accuracy, efficiency, and universality.

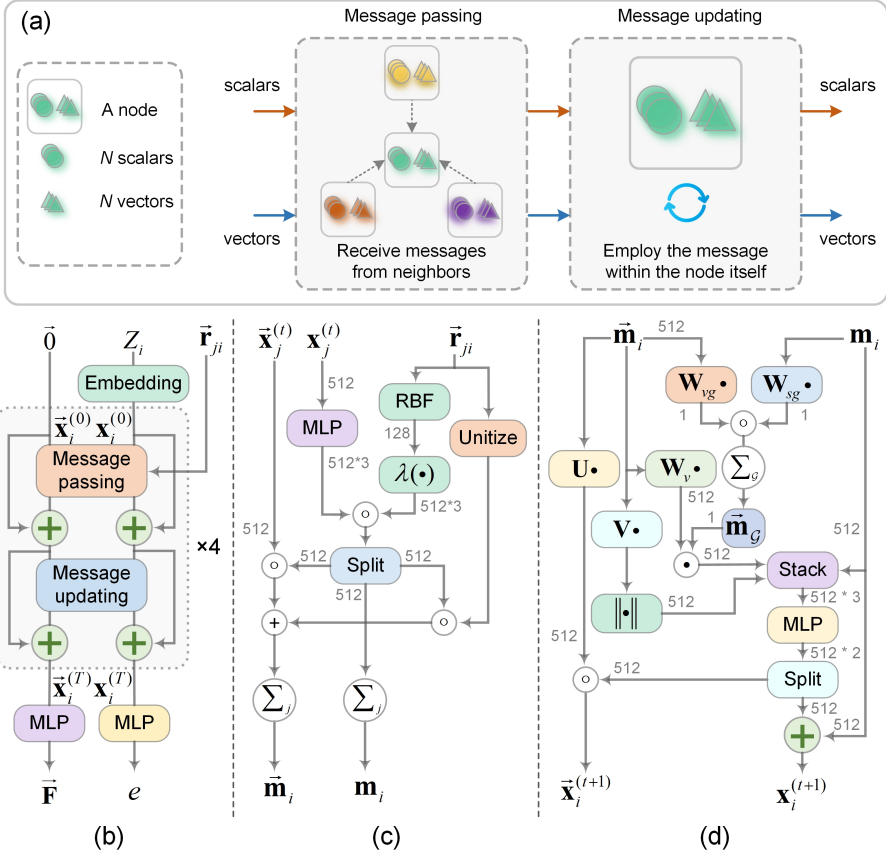


Fig. 2 The overall architecture of LEIGNN. (a) LEIGNN uses message passing and message updating to iteratively update node representations. (b) LEIGNN consists of four layers. (c) The message passing phase. (d) The message updating phase. The number of features after each operation is annotated in grey.

2 Results

2.1 Equivariant graph neural network

In this work, we enhance GNNs by incorporating equivariance, enabling an active exploration of symmetries and yielding a richer geometric representation. Each node in LEIGNN is assigned scalars and vectors to represent invariant and equivariant features, respectively. LEIGNN gradually updates the node representations through two key processes: message passing and message updating, as illustrated in Figure 2 (a). The message passing phase aims at aggregating neighboring nodes to mimic two-body interactions, whereas the message updating is used to integrate N scalars and N vectors within a node to update node representations. LEIGNN consists of four layers, each comprising two phases: message passing and message updating, as illustrated in Figures 2 (b) to (d) and elaborated in the **Method** section. The model’s efficiency is further augmented by a novel strategy for extracting global structural features from the vector representation. This strategy, detailed in the **Method** section, sets LEIGNN apart from previous models[36, 37], providing a unique approach to capturing global structural information.

Table 1 Comparison results of the proposed LEIGNN and baselines on S2EF task of four external validation sets of OC20 in terms of energy MAE (meV) and forces MAE (meV/Å), where all models are trained on the same OC20-50K. The ‘Improvement (%)’ row indicates the percentage by which LEIGNN outperforms the previous best model.

Model	ID		OOD Ads.		OOD Cat.		OOD Both	
	Energy	Forces	Energy	Forces	Energy	Forces	Energy	Forces
CGCNN	1125	75.3	1255	79.9	1111	74.4	1386	91.5
SchNet	1138	67.9	1255	73.3	1121	67.4	1394	84.9
PaiNN	680	66.6	877	72.1	671	66.2	973	83.3
DimeNet++	647	59.2	752	68.2	646	58.7	875	78.5
GemNet-dT	641	58.7	784	63.8	733	58.1	1029	75.4
LEIGNN (ours)	543	55.4	655	60.2	585	54.9	778	71.0
Improvement	15.3%	5.6%	12.9%	11.7%	12.8%	6.5%	11.1%	9.6%

2.2 Model performance

We first evaluate LEIGNN in the structure to energy and forces (S2EF) task using Open Catalyst 2020 (OC20) dataset[38]. The purpose of this task is to predict energies and forces corresponding to each trajectory during structural relaxation. The OC20 dataset encompasses 1,281,040 density functional theory (DFT) relaxations with 264,890,000 single-point calculations and spans a vast range of materials, surfaces, and adsorbates. It has been reported that training a GNN model on the whole OC20 dataset requires hundreds or even thousands of days [33]. Therefore, we only use a subset of it: OC20-50K ($N = 50,000$). The dataset is split into a training set and an internal validation set with a

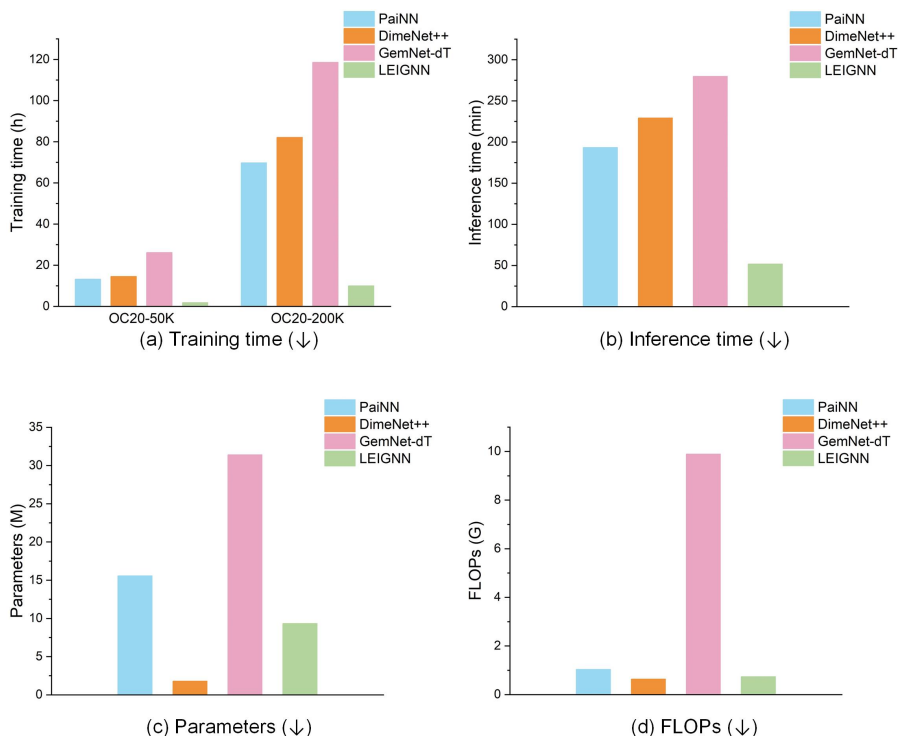


Fig. 3 Computational costs of the six models (the lower the better for all metrics). (a) Training time. (b) Mean inference time. (c) Number of parameters. (d) FLOPs.

ratio of 8:2, where the internal validation set is used to select the best model for testing. Finally, the select models are tested on four external validation sets provided by the OC20 project: in Domain (ID), out-of-domain adsorbate (OOD Ads.), out-of-domain catalyst (OOD Cat.), and OOD Both (both the adsorbate and catalyst are not seen in the training set). Each external validation set contains approximately 1M data points. We compare LEIGNN with five representative baseline models: CGCNN, SchNet, PaiNN, DimeNet++, and GemNet-dT. All models are implemented using the source code provided by Open Catalyst Project¹ with recommended hyper-parameters. All models share the same training, internal validation, and external validation sets, and are trained to predict adsorption energy and per-atom forces simultaneously. The performance of the models is evaluated based on the mean absolute error (MAE).

As shown in Table 1, LEIGNN consistently surpasses benchmark models in energy and force predictions across all external validation sets, especially the CGCNN and SchNet. LEIGNN’s implicit consideration of structural features can yield competitive performance compared to DimeNet++ and GemNet-dT which explicitly incorporate angular features. Furthermore, when evaluated

¹<https://github.com/Open-Catalyst-Project/ocp>

on a larger dataset, OC20-200K ($N = 200,000$), LEIGNN still demonstrates robust and competitive performance (Table S1).

Next, we compare the computational costs among LEIGNN and the three accurate models of PaiNN, DimeNet++, and GemNet-dT in Table 1. Figure 3 illustrates the model complexity in terms of training time, inference time, the number of parameters, and floating-point operations (FLOPs). As can be seen, LEIGNN offers approximately ten times faster training and inference speeds than GemNet-dT and is about five times faster than DimeNet++ and PaiNN. These findings highlight LEIGNN’s high efficiency. The lightweight feature of LEIGNN renders it a more suitable choice for large-scale simulation systems.

Besides the OC20 database, we compare LEIGNN and other models on MD17 and ISO17 databases. Our LEIGNN model also surpasses those benchmark models as shown in Tables S2 and S3.

Finally, to showcase the efficacy of our novel approach for extracting global structural features from the vector representation, we conduct a comparative analysis between LEIGNN and a baseline variant, denoted as LEIGNN_noG, which omits the integration of global structural information. The findings of this comparison are presented in Table S4, underscoring the significant role that global structure plays in our model’s performance.

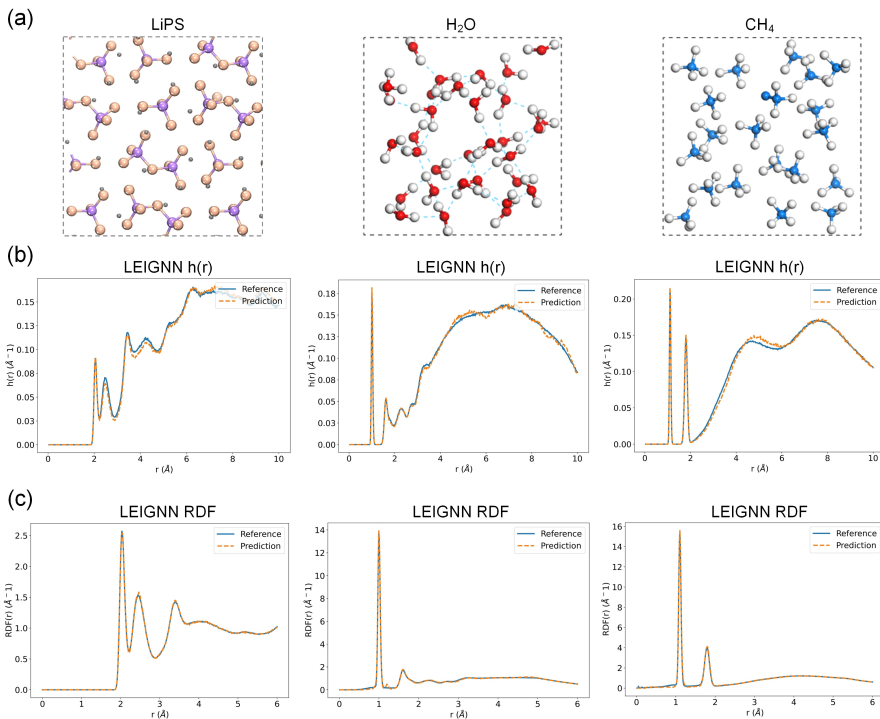


Fig. 4 MD simulations for LiPS, H₂O, and CH₄. (a) An overview of the three benchmark systems. (b) $h(r)$ for trajectories predicted by the LEIGNN. (c) RDF for trajectories predicted by LEIGNN.

2.3 Applying LEIGNN to molecular dynamics simulations

Molecular dynamics simulations provide vital atomistic insights, but the accuracy versus efficiency trade-off has long been a challenge. Classical MD, which relies on empirical interatomic potentials, is computationally efficient but sacrifices accuracy. In contrast, *ab initio* molecular dynamics, which integrates first-principles methods such as density functional theory, provides higher accuracy but at a significant computational cost.

As the validation of our LEIGNN’s interatomic potentials, we finally demonstrate that our LEIGNN can have the computational efficiency of classical MD while retaining the AIMD-level accuracy. We benchmark LEIGNN against the classical MD potentials, evaluating stability, MAE of interatomic distances ($h(r)$), MAE of radial distribution function (RDF), and running time. For a clear metric of stability, we deem simulations to be ‘unstable’ if deviations surpass predefined thresholds, indicating the sampling of highly nonphysical structures[35]. To test our model robustness, we consider various systems, including LiPS (solid), H₂O (liquid), and CH₄ (gas), as shown in Figure 4 (a), over a 50 ps simulation initiated from a randomly chosen test configuration. Refer to the **Method** section for detailed metrics and experimental settings.

Our results, summarized in Table 2, reveal LEIGNN’s superiority over classical MD in both stability and accuracy for all systems. LEIGNN maintains consistent stability throughout the 50 ps simulations and demonstrates notably low MAEs for $h(r)$ and RDF, suggesting its ability to accurately capture the structural properties of the system. Moreover, their running times are similar, highlighting LEIGNN’s efficiency.

We further compare LEIGNN with high-fidelity AIMD. Figures 4 (b), (c) shows the $h(r)$ and RDF for AIMD and LEIGNN, revealing their strong alignment. Additional results are presented in Figure S1. Overall, our results spotlight LEIGNN’s potential as a pivotal tool in computational materials science.

Table 2 Evaluating LEIGNN and the classical Lennard-Jones (LJ) potential on MD simulations in terms of stability (ps), MAE of $h(r)$ (unitless), MAE of RDF (unitless), and running time (min).

System	#Atoms	Method	Stability(↑)	$h(r)$ (↓)	RDF(↓)	Time
LiPS (solid)	83	Lennard-Jones	0	0.42	12.34	29.93
		LEIGNN (ours)	50	0.03	0.04	43.85
H2O (liquid)	96	Lennard-Jones	0	0.61	9.58	15.53
		LEIGNN (ours)	50	0.02	0.19	26.95
CH4 (gas)	100	Lennard-Jones	0	0.48	9.85	15.17
		LEIGNN (ours)	50	0.03	0.20	26.53

3 Conclusion

The prediction of energy and forces with high precision yet efficient time scale holds significant value in the exploration of chemical and material systems. We have developed a high-efficiency model, LEIGNN, to predict energy and forces by utilizing a vector representation to encode structural information, thereby circumventing the need for explicit angular feature computation. Unlike previous models which only consider local structural features contained in the vector representation, we propose an innovative approach to extract global structural features from the vector representation. We demonstrate that these global structural features are essential for energy prediction. By taking advantage of geometric message passing, LEIGNN archives equivariant atom-wise representations, enabling it to deliver remarkable accuracy without substantial computational or memory load. Experimental results on OC20, MD17, and ISO17 prove the superior performance and streamlined nature of LEIGNN. Furthermore, the superiority of LEIGNN in simulating physical and chemical behaviors is evidenced by molecular dynamics simulations on diverse systems. These simulations, driven by LEIGNN-calculated forces, accurately represent the structural properties of the tested systems. In essence, LEIGNN emerges as a potent tool, enabling more profound explorations in the realm of computational science, such as complex chemical, physical, and material systems. The key contributions of this work in the field of computational science are summarized as follows: 1) LEIGNN employs a scalar-vector dual representation, with vectors intrinsically embodying structural information of materials, thus eliminating the need for explicit calculation of chemical bond angles. This feature has demonstrated considerable improvement in terms of running time in molecular dynamics simulation. 2) LEIGNN introduces a novel way to extract global structural features from the vector representation. We demonstrate that this novel strategy can enhance the model performance greatly. 3) LEIGNN enforces the neural network to satisfy the symmetry constraints, thus bypassing the need for computationally expensive data augmentation strategies.

4 Method

4.1 Problem definition

In this work, the atomic structure is represented as a 3D interaction graph $\mathcal{G} = (\mathcal{V}, \mathcal{E}, \mathcal{R})$, where \mathcal{V} and \mathcal{E} are sets of nodes and edges. \mathcal{R} are sets of 3D coordinates of nodes. Each node is connected to its closest neighbors within a cutoff distance D with a maximum number of neighbors N , where D and N are predefined numbers. Each node $v_i \in \mathcal{V}$ has its scalar feature $\mathbf{x}_i \in \mathbb{R}^F$, vector feature $\vec{\mathbf{x}}_i \in \mathbb{R}^{F \times 3}$ (i.e., retaining F scalars and F vectors for each node), and 3D coordinate $\vec{\mathbf{r}}_i \in \mathbb{R}^3$. The scalar and vector features can be updated during training. We set the number of features F as a constant throughout the network. The scalar feature is initialized to an embedding only dependent on the atomic number as $\mathbf{x}_i^{(0)} = E(z_i) \in \mathbb{R}^F$, where z_i is the atomic number and E is an embedding layer that takes z_i as input and returns a F -dimensional feature. This embedding is similar to the one-hot vector but is trainable. The vector feature is set to $\vec{\mathbf{x}}_i^{(0)} = \vec{\mathbf{0}} \in \mathbb{R}^{F \times 3}$ at the initial step. We also define $\vec{\mathbf{r}}_{ij} = \vec{\mathbf{r}}_j - \vec{\mathbf{r}}_i$ as a vector from node v_i to node v_j . Norm $\|\cdot\|$ and dot product \cdot are calculated along the spatial dimension, while concatenation \oplus and Hadamard product \circ are calculated along the feature dimension. Given a set of 3D interaction graphs, our goal is to learn a model f to predict the potentials and forces as $f(\mathcal{G}) = (e, \vec{\mathbf{F}})$, where $e \in \mathbb{R}^1$, $\vec{\mathbf{F}} \in \mathbb{R}^{M \times 3}$ and M is the number of nodes in \mathcal{G} .

4.2 Lightweight equivariant interaction graph neural network

LEIGNN iteratively updates the representation of a node through a two-phase process: message passing and message updating as shown in Figure 2. During the message passing phase, a node can receive messages from its neighboring nodes, which progressively expands its accessible radius. In the message updating phase, LEIGNN only employs the message within the node itself (a node has F scalars and F vectors) to update node features (Figure 5).

4.2.1 Message passing phase

In the message passing phase, a particular node v_i gathers messages from its neighbouring scalar \mathbf{x}_j and vector $\vec{\mathbf{x}}_j$, resulting in intermediate scalar and vector variables \mathbf{m}_i and $\vec{\mathbf{m}}_i$ as follows:

$$\mathbf{m}_i = \sum_{v_j \in \mathcal{N}(v_i)} (\mathbf{W}_h \mathbf{x}_j^{(t)}) \circ \lambda_h(\|\vec{\mathbf{r}}_{ji}\|) \quad (1)$$

$$\vec{\mathbf{m}}_i = \sum_{v_j \in \mathcal{N}(v_i)} (\mathbf{W}_u \mathbf{x}_j^{(t)}) \circ \lambda_u(\|\vec{\mathbf{r}}_{ji}\|) \circ \vec{\mathbf{x}}_j^{(t)} + (\mathbf{W}_v \mathbf{x}_j^{(t)}) \circ \lambda_v(\|\vec{\mathbf{r}}_{ji}\|) \circ \frac{\vec{\mathbf{r}}_{ji}}{\|\vec{\mathbf{r}}_{ji}\|} \quad (2)$$

Here, $\mathbf{W}_h, \mathbf{W}_u, \mathbf{W}_v \in \mathbb{R}^{F \times F}$ are learnable matrices. The functions $\lambda_h, \lambda_u,$ and λ_v are the linear combination of Gaussian radial basis functions (RBF)[6]. For the Eqn. (2), the first term $(\mathbf{W}_u \mathbf{x}_j^{(t)}) \circ \lambda_u(\|\vec{\mathbf{r}}_{ji}\|) \circ \vec{\mathbf{x}}_j^{(t)}$ propagates directional information $\mathbf{x}_j^{(t)}$ obtained in the previous step to neighboring atoms, with $(\mathbf{W}_u \mathbf{x}_j^{(t)}) \circ \lambda_u(\|\vec{\mathbf{r}}_{ji}\|)$ acting as a gate signal to control how many signals in the previous step can be preserved. We interpret the second term as the force exerted by atom j on atom i , where $(\mathbf{W}_v \mathbf{x}_j^{(t)}) \circ \lambda_v(\|\vec{\mathbf{r}}_{ji}\|)$ is force magnitude and $\frac{\vec{\mathbf{r}}_{ji}}{\|\vec{\mathbf{r}}_{ji}\|}$ is the force direction. This is conceptually different from PaiNN's message function, which uses $\vec{\mathbf{r}}_{ij}$ instead of $\vec{\mathbf{r}}_{ji}$. Subsequently, $\sum_{v_j \in \mathcal{N}(v_i)} (\mathbf{W}_v \mathbf{x}_j^{(t)}) \circ \lambda_v(\|\vec{\mathbf{r}}_{ji}\|) \circ \frac{\vec{\mathbf{r}}_{ji}}{\|\vec{\mathbf{r}}_{ji}\|}$ represents the total force exerted on atom i and is a linear combination of forces exerted on it by all other atoms. It is noteworthy that we retain F vectors for each node, which means that the forces are calculated F times in parallel to provide more extensive vector representations. Figure 5 (a) shows an example of how the F forces are calculated.

4.2.2 Message updating phase

The message updating phase aims to aggregate F scalars and vectors within \mathbf{m}_i and $\vec{\mathbf{m}}_i$, respectively, to obtain new scalar $\mathbf{x}_i^{(t+1)}$ and new vector $\vec{\mathbf{x}}_i^{(t+1)}$. Figure 5 (b) shows an example of how to aggregate F vectors within $\vec{\mathbf{m}}_i$. Two strategies are employed to extract the local and global structures from the $\vec{\mathbf{m}}_i$. The local structure is extracted using vector norm $\|\mathbf{V} \vec{\mathbf{m}}_i\|$ ($\mathbf{V} \in \mathbb{R}^{F \times F}$), while the global structure is obtained by projecting each vector onto a global vector. Specifically, we first define the global vector $\vec{\mathbf{m}}_G$ as follows:

$$\vec{\mathbf{m}}_G = \sum_{v_i \in \mathcal{G}} (\mathbf{W}_{sg} \mathbf{m}_i) \circ (\mathbf{W}_{vg} \vec{\mathbf{m}}_i) \quad (3)$$

where $\mathbf{W}_{sg} \in \mathbb{R}^{1 \times F}$ and $\mathbf{W}_{vg} \in \mathbb{R}^{1 \times F}$ are two learnable matrices compressing \mathbf{m}_i and $\vec{\mathbf{m}}_i$ to a scalar and a three-dimensional vector, respectively. $\vec{\mathbf{m}}_G \in \mathbb{R}^3$ is a global vector encoding the global structural information. We then use $\vec{\mathbf{m}}_G$ as a reference coordinate system and project each local vector onto it.

$$\mathbf{s} = (\mathbf{W}_v \vec{\mathbf{m}}_i) \cdot \vec{\mathbf{m}}_G \quad (4)$$

where $\mathbf{W}_v \in \mathbb{R}^{F \times F}$, $\mathbf{s} \in \mathbb{R}^F$ is the extracted global structure. Therefore, by projecting each local vector $\vec{\mathbf{m}}_i$ onto the global vector $\vec{\mathbf{m}}_G$, both the magnitude and angular information are implicitly extracted. Figure 5 (c) shows an example of how to calculate the global vector and how to project each local vector onto it. Finally, the scalar representation $\mathbf{x}_i^{(t+1)}$ and vector representation $\vec{\mathbf{x}}_i^{(t+1)}$ is updated according to:

$$\mathbf{x}_i^{(t+1)} = \mathbf{W}_{u1}(\mathbf{m}_i \oplus \|\mathbf{V} \vec{\mathbf{m}}_i\| \oplus \mathbf{s}) + \mathbf{W}_{u2} \mathbf{m}_i \quad (5)$$

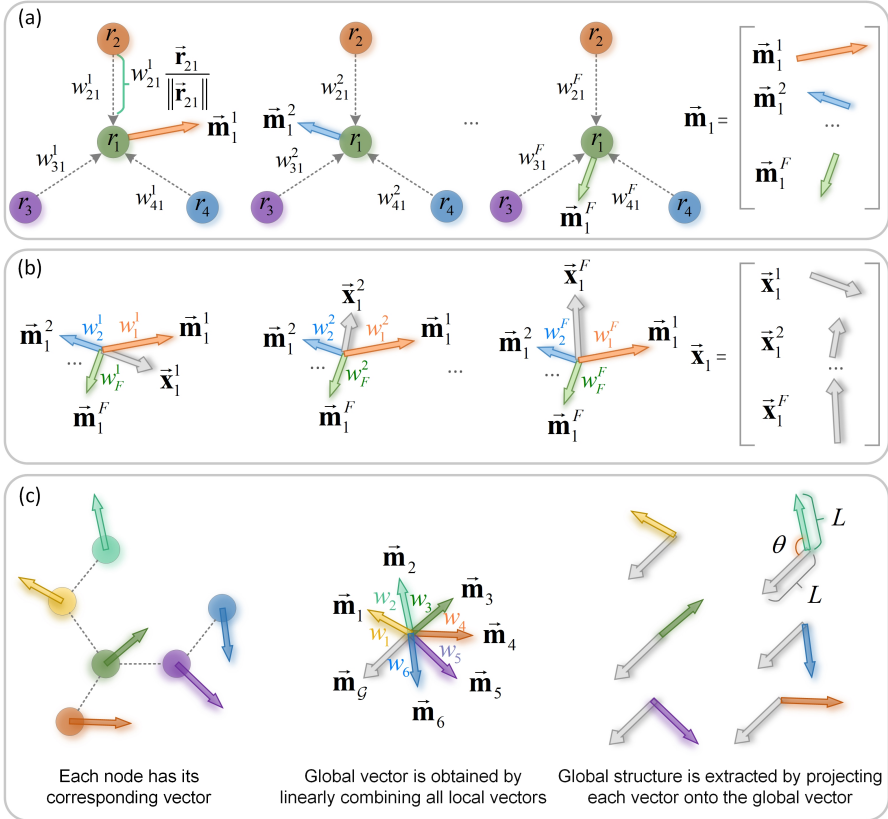


Fig. 5 An illustration of how vector representation evolves during message passing phase and message updating phase. (a) An example explains how to calculate the intermediate vector representation $\vec{\mathbf{m}}_1$. For the sake of simplicity, we ignore the first term of Eqn (2). The f -th vector in $\vec{\mathbf{m}}_1$ (i.e., $\vec{\mathbf{m}}_1^f$) can be interpreted as the force exerted by neighboring atom j on atom 1, where w_{j1}^f is force magnitude and $\frac{\vec{\mathbf{r}}_{j1}}{\|\vec{\mathbf{r}}_{j1}\|}$ is the force direction. Subsequently, the total force exerted on atom 1 is a linear combination of forces exerted on it by all other neighboring atoms j . Note that the forces are calculated F times in parallel. (b) The update to $\vec{\mathbf{x}}_1$ is achieved through a linear combination of F vectors within $\vec{\mathbf{m}}_1$. This computation is performed in parallel F times to obtain $\vec{\mathbf{x}}_1$. (c) An example explains how to project each local vector to the global vector via dot product.

$$\vec{\mathbf{x}}_i^{(t+1)} = (\mathbf{W}_h(\mathbf{m}_i \oplus \|\mathbf{V}\vec{\mathbf{m}}_i\| \oplus \mathbf{s})) \circ (\mathbf{U}\vec{\mathbf{m}}_i) \quad (6)$$

where \oplus is concatenation, $\mathbf{W}_{u1}, \mathbf{W}_h \in \mathbb{R}^{F \times 3F}$ and $\mathbf{W}_{u2}, \mathbf{U}, \mathbf{V} \in \mathbb{R}^{F \times F}$.

4.2.3 Predicting potentials and forces

To predict the potential e , we utilize an MLP layer $\phi: \mathbb{R}^F \rightarrow \mathbb{R}^1$. This layer learns atom-wise potentials $e_i \in \mathbb{R}^1$ from the scalar representation $\mathbf{x}_i^{(T)}$ which is obtained at the last graph convolution layer (referred to as the T -th layer). The total potential is then calculated as the sum of the atom-wise potentials:

$$e = \sum_{v_i \in \mathcal{G}} e_i \quad (7)$$

On the other hand, the forces are predicted using the vector representation $\vec{\mathbf{x}}_i^{(T)}$ as $\vec{\mathbf{F}} = \mathbf{W}_f \vec{\mathbf{x}}_i^{(T)}$, where $\mathbf{W}_f \in \mathbb{R}^{1 \times F}$. Notably, this differs from the approaches employed by PaiNN[36] and NewtonNet[37], where forces are computed by differentiating the predicted energy with respect to the atom positions, i.e., $\vec{\mathbf{F}} = \frac{\partial e}{\partial \mathbf{r}}$. Such differentiation incurs additional computational costs.

4.3 Implementation details

The LEIGNN comprises four layers, with each layer consisting of two phases: message passing and message updating, as illustrated in Figure 2 (b). To prevent over-smoothing[39, 40], skip connections are added to each layer. The process of message passing and message updating is elaborated in Figures 2 (c) and (d) respectively.

The LEIGNN model is implemented using PyTorch. Experiments are conducted on an NVIDIA GeForce RTX A4000 with 16 GB of memory. The training objective aims to minimize the loss function defined as:

$$\mathcal{L} = \frac{1}{N} \sum_{n=1}^N \left(\alpha |e_n - e_n^l| + \beta \frac{1}{3M} \sum_{m=1}^M \sum_{k=1}^3 |\vec{\mathbf{F}}_{nmk} - \vec{\mathbf{F}}_{nmk}^l| \right) \quad (8)$$

where e_n^l represents the ground truth energy of n -th sample, $\vec{\mathbf{F}}_{nmk}^l$ is the ground truth force of k -th dimension of m -th atom in n -th sample. The variables N and M denote the sample size and the number of atoms in each sample, and α and β denote the weights assigned to the energy and force losses, respectively.

For other baselines, we employ the recommended hyperparameters provided by the OCP² and MDsim³ source codes for the OC20 and MD17 datasets, respectively.

4.4 Proof of invariance and equivalence

First, it can be easily verified that the predicted scalar potentials of LEIGNN exhibit invariance to translations and rotations. Specifically, the initial scalar feature $\mathbf{x}_i^{(0)}$ is invariant, and the update process of $\mathbf{x}_i^{(t)}$ solely relies on invariant operations, such as vector norm and dot product. Therefore, the predicted potentials of LEIGNN are invariant. On the other hand, the predicted vector forces are multiple linear combinations of unit vectors $\frac{\vec{\mathbf{r}}_{ji}}{\|\vec{\mathbf{r}}_{ji}\|}$, which are equivalent. A formal proof is as follows.

²<https://github.com/Open-Catalyst-Project/ocp>

³<https://github.com/kyonofx/MDsim>

Let $\vec{\mathbf{g}} \in \mathbb{R}^3$ be a translation vector and $\mathbf{Q} \in \mathbb{R}^{3 \times 3}$ be a unitary rotation matrix. We prove that the vector representations are invariant to the translations and equivariant to rotations. Since both translation and rotation do not affect the values of $\|\cdot\|$ or dot product, we can view them as scalars (i.e., invariant features). We then consider $\vec{\mathbf{m}}_i$ as a function of $\vec{\mathbf{x}}_i$, $\vec{\mathbf{x}}_j$ and $\vec{\mathbf{r}}_{ji}$, that is $\vec{\mathbf{m}}_i = \phi(\vec{\mathbf{x}}_i, \vec{\mathbf{x}}_j, \vec{\mathbf{r}}_{ji})$. Note that $\vec{\mathbf{r}}_{ji} = \vec{\mathbf{r}}_i - \vec{\mathbf{r}}_j$.

Invariance. Note that $(\vec{\mathbf{r}}_i + \vec{\mathbf{g}}) - (\vec{\mathbf{r}}_j + \vec{\mathbf{g}}) = \vec{\mathbf{r}}_i - \vec{\mathbf{r}}_j$. Therefore, the output $\vec{\mathbf{m}}_i$ will be invariant to translation as

$$\vec{\mathbf{m}}_i = \phi(\vec{\mathbf{x}}_i, \vec{\mathbf{x}}_j, (\vec{\mathbf{r}}_i + \vec{\mathbf{g}}) - (\vec{\mathbf{r}}_j + \vec{\mathbf{g}})) = \phi(\vec{\mathbf{r}}_{ij}, \vec{\mathbf{x}}_i, \vec{\mathbf{r}}_{ji}) \quad (9)$$

Since $\vec{\mathbf{x}}_i^{(t+1)}$ only depends on $\vec{\mathbf{m}}_i$ and scalars $\mathbf{m}_i \oplus \|\mathbf{V}\vec{\mathbf{m}}_i\| \oplus \mathbf{s}$ (\mathbf{s} is global structural features and is invariant), we can conclude that the vector representations are invariant to translations.

Equivalence. Suppose $t = 0$ and note that $\vec{\mathbf{x}}_i^{(0)} = \vec{\mathbf{0}} \in \mathbb{R}^{F \times 3}$, we then have $\vec{\mathbf{m}}_i = \sum_{v_j \in \mathcal{N}(v_i)} \mathbf{W}_v \mathbf{x}_j^{(0)} \circ \vec{\mathbf{r}}_{ji}$ (we ignore $\|\vec{\mathbf{r}}_{ji}\|$ for simplicity). Note that Hadamard product (i.e., \circ) can be viewed as left multiplication by a diagonal matrix \mathbf{D} . Therefore, we can rewrite Eqn. (6) as

$$\vec{\mathbf{x}}_i^{(1)} = \mathbf{D}_h \mathbf{U} \sum_{v_j \in \mathcal{N}(v_i)} \mathbf{D}_v (\vec{\mathbf{r}}_i - \vec{\mathbf{r}}_j) \quad (10)$$

where $\mathbf{D}_v = \mathbf{W}_v \mathbf{x}_j^{(t)}$ and $\mathbf{D}_h = \mathbf{W}_h (\mathbf{m}_i \oplus \|\mathbf{V}\vec{\mathbf{m}}_i\| \oplus \mathbf{s})$. Here, we consider the coordinates as a set of row vectors. Therefore, rotating the coordinates \mathcal{R} can be achieved by multiplication with \mathbf{Q} from the right. Thus, $\vec{\mathbf{x}}_i^{(1)}$ will be equivalent to rotation as

$$\begin{aligned} \vec{\mathbf{x}}_i^{(1)} &= \mathbf{D}_h \mathbf{U} \sum_{v_j \in \mathcal{N}(v_i)} \mathbf{D}_v (\vec{\mathbf{r}}_i \mathbf{Q} - \vec{\mathbf{r}}_j \mathbf{Q}) \\ &= [\mathbf{D}_h \mathbf{U} \sum_{v_j \in \mathcal{N}(v_i)} \mathbf{D}_v (\vec{\mathbf{r}}_i - \vec{\mathbf{r}}_j)] \mathbf{Q} \end{aligned} \quad (11)$$

We can conclude $\vec{\mathbf{x}}_i^{(1)}$ is equivalent to rotation. Now suppose $\vec{\mathbf{x}}_i^{(t)}$ is already equivalent to rotation. Again, we can rewrite Eqn. (6) as

$$\vec{\mathbf{x}}_i^{(t+1)} = \mathbf{D}_h \mathbf{U} \sum_{v_j \in \mathcal{N}(v_i)} \mathbf{D}_u \vec{\mathbf{x}}_j^{(t)} + \mathbf{D}_v (\vec{\mathbf{r}}_i - \vec{\mathbf{r}}_j) \quad (12)$$

where $\mathbf{D}_u = \mathbf{W}_u \mathbf{x}_j^{(t)}$. Similarly, we have

$$\vec{\mathbf{x}}_i^{(t+1)} = \mathbf{D}_h \mathbf{U} \sum_{v_j \in \mathcal{N}(v_i)} \mathbf{D}_u \vec{\mathbf{x}}_j^{(t)} \mathbf{Q} + \mathbf{D}_v (\vec{\mathbf{r}}_i \mathbf{Q} - \vec{\mathbf{r}}_j \mathbf{Q})$$

$$= [\mathbf{D}_h \mathbf{U} \sum_{v_j \in \mathcal{N}(v_i)} \mathbf{D}_u \bar{\mathbf{x}}_j^{(t)} + \mathbf{D}_v (\bar{\mathbf{r}}_i - \bar{\mathbf{r}}_j)] \mathbf{Q} \quad (13)$$

Therefore, we can claim that the vector representations are equivalent to rotations.

4.5 Datasets for MD simulations

4.5.1 Solid LiPS

In this simulation, we use $\text{Li}_{6.75}\text{P}_3\text{S}_{11}$, a crystalline superionic lithium conductor widely used in battery development. The simulation cell comprises 83 atoms and serves as a representative system for studying kinetic properties in materials through MD simulations. We utilize the dataset from Batzner et al.’s work[14]. This AIMD trajectory consists of a total of 25,000 structures, with 19,000 randomly sampled structures used for training, 1,000 for validation, and the remainder for testing. The simulation employs a time step of 0.25 fs and a temperature of 520 K, with a Nosé–Hoover thermostat.

4.5.2 Liquid H₂O

Water, essential in biological and chemical processes, presents complexities in thermodynamics and phase behavior that make it challenging to simulate. For this system, our dataset comprises 100,000 structures. Of these, 72,000 structures are randomly sampled for training, 8,000 for validation, and the remaining 20,000 for testing. The simulation is set with a time step of 0.5 fs, a temperature of 300 K, and uses a Langevin thermostat. The duration of the simulation is 50 ps.

4.5.3 Gas CH₄

Methane is a potent greenhouse gas with significant implications for climate change and serves as the primary component of natural gas, a vital global energy source. Its molecular dynamics properties are crucial for understanding environmental impacts, energy applications, and broader scientific phenomena. For methane, our dataset is made up of 100,000 structures. From this, 72,000 structures are randomly sampled for training, 8,000 for validation, and the remaining 20,000 for testing. The simulation adopts a time step of 0.5 fs, a temperature of 300 K, and a Langevin thermostat. The simulation’s duration is set at 50 ps.

The test results for the three systems, measured in terms of energy and forces MAE, can be found in Table S5.

4.5.4 LEIGNN for MD simulations

We incorporate LEIGNN-based forces with the Atomic Simulation Environment (ASE)[41] to perform MD simulations. For the LiPS system, we use a

Nosé-Hoover thermostat, while for water and methane, we opt for a Langevin thermostat. The parameters are consistent with those from the AIMD run.

4.6 Performance indicators

Mean absolute error (MAE). The performance of energy and force predictions is quantified using MAE, calculated as follows:

$$\text{MAE}(e) = \frac{1}{N} \sum_{n=1}^N |e_n - e_n^l| \quad (14)$$

$$\text{MAE}(\vec{\mathbf{F}}) = \frac{1}{3NM} \sum_{n=1}^N \sum_{m=1}^M \sum_{k=1}^3 |\vec{\mathbf{F}}_{nmk} - \vec{\mathbf{F}}_{nmk}^l| \quad (15)$$

Distribution of interatomic distances. The distribution of interatomic distances ($h(r)$) offers a concise representation of a system's 3D structure and has been explored in prior research [35, 42]. For a specific configuration denoted as x , $h(r)$ is determined using the equation:

$$h(r) = \frac{1}{N(N-1)} \sum_i^N \sum_{j \neq i}^N \delta(r - \|x_i - x_j\|) \quad (16)$$

In this equation, r represents the distance from a reference particle, while N denotes the total particle count. The indices i and j identify the atom pairs contributing to the distance statistics. The function δ is the Dirac Delta function, employed to extract value distributions. To determine the ensemble average, $h(r)$ is computed and then averaged across frames.

Radial distribution function (RDF). RDF, a valuable simulation observable, characterizes the structural and thermodynamic properties of the system. By its definition, the RDF elucidates the variation of density as a function of distance from a reference particle. The RDF for a particular configuration x is computed as follows:

$$\text{RDF}(r) = \frac{1}{4\pi r^2} \frac{1}{N\rho} \sum_{i=1}^N \sum_{j \neq i}^N \delta(r - \|x_i - x_j\|) \quad (17)$$

In this equation, r represents the distance from a reference particle, N is the total number of particles, and i, j are indices referring to the atom pairs contributing to distance statistics. Additionally, ρ denotes the system's density, and δ is the Dirac Delta function, applied for value distribution extraction. The ensemble average is calculated by averaging $\text{RDF}(r)$ over frames. The

final RDF MAE is obtained by integrating over r :

$$\text{MAE(RDF)} = \int_{r=0}^{\infty} |\langle \text{RDF}(r) \rangle - \langle \hat{\text{RDF}}(r) \rangle| dr \quad (18)$$

where $\langle \cdot \rangle$ indicates the averaging operator, $\langle \text{RDF}(r) \rangle$ is the reference equilibrium RDF, and $\langle \hat{\text{RDF}}(r) \rangle$ is the RDF predicted by the model.

Stability criterion. In the study, stability is defined as the ability to retain low-energy configurations[35]. For systems with periodic boundary conditions, we monitor stability by tracking equilibrium statistics. We denote a simulation as ‘unstable’ at time T if

$$\int_{r=0}^{\infty} \|\langle \text{RDF}(r) \rangle - \langle \hat{\text{RDF}}(r) \rangle_{t=T}^{T+\tau}\| dr > \Delta \quad (19)$$

where τ refers to a short time window and Δ represents the stability threshold. We set $\Delta = 1.0$, which is the same as in MDsim[35]. The stability of a model is subsequently assessed based on how long it maintains stability during the simulation.

Code availability

Data and code for LEIGNN are available at <https://github.com/guaguabujianle/LEIGNN>.

Author Contributions

Lei Shen and Ziduo Yang designed the research. Ziduo Yang and Xian Wang worked together to conduct the experiment. Ziduo Yang, Xian Wang, Yifan Li, Qiuji Lv, Calvin Yu-Chian Chen, and Lei Shen analyzed the data and results. Ziduo Yang and Lei Shen wrote the manuscript together.

Conflicts of interest

The authors declare that they have no competing interests.

Acknowledgements

This work was supported by the National Natural Science Foundation of China (Grant No. 62176272), Research and Development Program of Guangzhou Science and Technology Bureau (No. 2023B01J1016), Key-Area Research and Development Program of Guangdong Province (No. 2020B1111100001).

References

- [1] Gasteiger, J., Becker, F., Günnemann, S.: Gemnet: Universal directional graph neural networks for molecules. *Advances in Neural Information Processing Systems* **34**, 6790–6802 (2021)
- [2] Li, H., Wang, Z., Zou, N., Ye, M., Xu, R., Gong, X., Duan, W., Xu, Y.: Deep-learning density functional theory hamiltonian for efficient ab initio electronic-structure calculation. *Nature Computational Science* **2**(6), 367–377 (2022)
- [3] Zhong, Y., Yu, H., Su, M., Gong, X., Xiang, H.: Transferable equivariant graph neural networks for the hamiltonians of molecules and solids. *npj Computational Materials* **9**(1), 182 (2023)
- [4] Xie, T., Grossman, J.C.: Crystal graph convolutional neural networks for an accurate and interpretable prediction of material properties. *Physical review letters* **120**(14), 145301 (2018)
- [5] Park, C.W., Wolverton, C.: Developing an improved crystal graph convolutional neural network framework for accelerated materials discovery. *Physical Review Materials* **4**(6), 063801 (2020)
- [6] Schütt, K., Kindermans, P.-J., Sauceda Felix, H.E., Chmiela, S., Tkatchenko, A., Müller, K.-R.: Schnet: A continuous-filter convolutional neural network for modeling quantum interactions. *Advances in neural information processing systems* **30** (2017)
- [7] Chen, C., Ye, W., Zuo, Y., Zheng, C., Ong, S.P.: Graph networks as a universal machine learning framework for molecules and crystals. *Chemistry of Materials* **31**(9), 3564–3572 (2019)
- [8] Gasteiger, J., Groß, J., Günnemann, S.: Directional message passing for molecular graphs. In: *International Conference on Learning Representations (ICLR)* (2020)
- [9] Choudhary, K., DeCost, B.: Atomistic line graph neural network for improved materials property predictions. *npj Computational Materials* **7**(1), 185 (2021)
- [10] Chen, C., Ong, S.P.: A universal graph deep learning interatomic potential for the periodic table. *Nature Computational Science* **2**(11), 718–728 (2022)
- [11] Deng, B., Zhong, P., Jun, K., Riebesell, J., Han, K., Bartel, C.J., Ceder, G.: Chgnet as a pretrained universal neural network potential for charge-informed atomistic modelling. *Nature Machine Intelligence*, 1–11 (2023)

- [12] Unke, O.T., Chmiela, S., Gastegger, M., Schütt, K.T., Sauceda, H.E., Müller, K.-R.: Spookynet: Learning force fields with electronic degrees of freedom and nonlocal effects. *Nature communications* **12**(1), 7273 (2021)
- [13] Pablo-García, S., Morandi, S., Vargas-Hernández, R.A., Jorner, K., Ivković, Ž., López, N., Aspuru-Guzik, A.: Fast evaluation of the adsorption energy of organic molecules on metals via graph neural networks. *Nature Computational Science*, 1–10 (2023)
- [14] Batzner, S., Musaelian, A., Sun, L., Geiger, M., Mailoa, J.P., Kornbluth, M., Molinari, N., Smidt, T.E., Kozinsky, B.: E (3)-equivariant graph neural networks for data-efficient and accurate interatomic potentials. *Nature communications* **13**(1), 2453 (2022)
- [15] Banik, S., Dhabal, D., Chan, H., Manna, S., Cherukara, M., Molinero, V., Sankaranarayanan, S.K.: Cegann: Crystal edge graph attention neural network for multiscale classification of materials environment. *npj Computational Materials* **9**(1), 23 (2023)
- [16] Unke, O.T., Meuwly, M.: Physnet: A neural network for predicting energies, forces, dipole moments, and partial charges. *Journal of chemical theory and computation* **15**(6), 3678–3693 (2019)
- [17] Wang, L., Liu, Y., Lin, Y., Liu, H., Ji, S.: Comenet: Towards complete and efficient message passing for 3d molecular graphs. *Advances in Neural Information Processing Systems* **35**, 650–664 (2022)
- [18] Zhang, X., Zhou, J., Lu, J., Shen, L.: Interpretable learning of voltage for electrode design of multivalent metal-ion batteries. *npj Computational Materials* **8**(1), 175 (2022)
- [19] Gilmer, J., Schoenholz, S.S., Riley, P.F., Vinyals, O., Dahl, G.E.: Neural message passing for quantum chemistry. In: *International Conference on Machine Learning*, pp. 1263–1272 (2017). PMLR
- [20] Louis, S.-Y., Zhao, Y., Nasiri, A., Wang, X., Song, Y., Liu, F., Hu, J.: Graph convolutional neural networks with global attention for improved materials property prediction. *Physical Chemistry Chemical Physics* **22**(32), 18141–18148 (2020)
- [21] Fuchs, F., Worrall, D., Fischer, V., Welling, M.: Se (3)-transformers: 3d roto-translation equivariant attention networks. *Advances in neural information processing systems* **33**, 1970–1981 (2020)
- [22] Brandstetter, J., Hesselink, R., van der Pol, E., Bekkers, E.J., Welling, M.: Geometric and physical quantities improve e (3) equivariant message passing. In: *International Conference on Learning Representations* (2021)

- [23] Satorras, V.G., Hoogeboom, E., Welling, M.: E (n) equivariant graph neural networks. In: International Conference on Machine Learning, pp. 9323–9332 (2021). PMLR
- [24] Dai, M., Demirel, M.F., Liang, Y., Hu, J.-M.: Graph neural networks for an accurate and interpretable prediction of the properties of polycrystalline materials. *npj Computational Materials* **7**(1), 103 (2021)
- [25] Omeel, S.S., Louis, S.-Y., Fu, N., Wei, L., Dey, S., Dong, R., Li, Q., Hu, J.: Scalable deeper graph neural networks for high-performance materials property prediction. *Patterns* (2022)
- [26] Wu, J., Yang, J., Liu, Y.-J., Zhang, D., Yang, Y., Zhang, Y., Zhang, L., Liu, S., *et al.*: Universal interatomic potential for perovskite oxides. *Physical Review B* **108**(18), 180104 (2023)
- [27] Dong, T., Yang, Z., Zhou, J., Chen, C.Y.-C.: Equivariant flexible modeling of the protein–ligand binding pose with geometric deep learning. *Journal of Chemical Theory and Computation* (2023)
- [28] Liu, Y., Wang, L., Liu, M., Lin, Y., Zhang, X., Oztekin, B., Ji, S.: Spherical message passing for 3d molecular graphs. In: International Conference on Learning Representations (ICLR) (2022)
- [29] Atz, K., Grisoni, F., Schneider, G.: Geometric deep learning on molecular representations. *Nature Machine Intelligence* **3**(12), 1023–1032 (2021)
- [30] Shuaibi, M., Kolluru, A., Das, A., Grover, A., Sriram, A., Ulissi, Z., Zitnick, C.L.: Rotation invariant graph neural networks using spin convolutions. *arXiv preprint arXiv:2106.09575* (2021)
- [31] Batzner, S., Musaelian, A., Kozinsky, B.: Advancing molecular simulation with equivariant interatomic potentials. *Nature Reviews Physics*, 1–2 (2023)
- [32] Musaelian, A., Batzner, S., Johansson, A., Sun, L., Owen, C.J., Kornbluth, M., Kozinsky, B.: Learning local equivariant representations for large-scale atomistic dynamics. *Nature Communications* **14**(1), 579 (2023)
- [33] Passaro, S., Zitnick, C.L.: Reducing so (3) convolutions to so (2) for efficient equivariant gnns. *arXiv preprint arXiv:2302.03655* (2023)
- [34] Zitnick, C.L., Das, A., Kolluru, A., Lan, J., Shuaibi, M., Sriram, A., Ulissi, Z., Wood, B.: Spherical Channels for Modeling Atomic Interactions. In: *Advances in Neural Information Processing Systems (NeurIPS)* (2022)

- [35] Fu, X., Wu, Z., Wang, W., Xie, T., Keten, S., Gomez-Bombarelli, R., Jaakkola, T.S.: Forces are not enough: Benchmark and critical evaluation for machine learning force fields with molecular simulations. *Transactions on Machine Learning Research* (2023)
- [36] Schütt, K., Unke, O., Gastegger, M.: Equivariant message passing for the prediction of tensorial properties and molecular spectra. In: *International Conference on Machine Learning*, pp. 9377–9388 (2021). PMLR
- [37] Haghightalari, M., Li, J., Guan, X., Zhang, O., Das, A., Stein, C.J., Heidar-Zadeh, F., Liu, M., Head-Gordon, M., Bertels, L., *et al.*: Newtonnet: A newtonian message passing network for deep learning of interatomic potentials and forces. *Digital Discovery* **1**(3), 333–343 (2022)
- [38] Chanussot, L., Das, A., Goyal, S., Lavril, T., Shuaibi, M., Riviere, M., Tran, K., Heras-Domingo, J., Ho, C., Hu, W., *et al.*: Open catalyst 2020 (oc20) dataset and community challenges. *Acs Catalysis* **11**(10), 6059–6072 (2021)
- [39] Yang, Z., Zhong, W., Lv, Q., Chen, C.Y.-C.: Learning size-adaptive molecular substructures for explainable drug–drug interaction prediction by substructure-aware graph neural network. *Chemical Science* **13**(29), 8693–8703 (2022)
- [40] Yang, Z., Zhong, W., Zhao, L., Chen, C.Y.-C.: Mgraphdta: deep multi-scale graph neural network for explainable drug–target binding affinity prediction. *Chemical science* **13**(3), 816–833 (2022)
- [41] Larsen, A.H., Mortensen, J.J., Blomqvist, J., Castelli, I.E., Christensen, R., Dulak, M., Friis, J., Groves, M.N., Hammer, B., Hargus, C., *et al.*: The atomic simulation environment—a python library for working with atoms. *Journal of Physics: Condensed Matter* **29**(27), 273002 (2017)
- [42] Zhang, L., Han, J., Wang, H., Car, R., Weinan, E.: Deep potential molecular dynamics: a scalable model with the accuracy of quantum mechanics. *Physical review letters* **120**(14), 143001 (2018)